Estuarine, Coastal and Shelf Science (1989) **29**, 549–571

Modelling Tidal Energetics of the Columbia River Estuary

B. S. Giese and D. A. Jay

School of Oceanography, University of Washington, Seattle, WA 98195, and Geophysics Program, University of Washington, Seattle, WA 98195, U.S.A.

Received 15 March 1988 and in revised form 27 June 1989

Keywords: tidal estuaries; tidal friction; numerical model; Columbia River Estuary

The Columbia River Estuary is shallow and has a mixed diurnal and semidiurnal tide, strong riverflow, broad tidal flats and variable channel cross-section. It is weakly non-linear with respect to tidal forcing, as measured by a ratio of tidal amplitude to depth. These features, common to many shallow estuaries, were incorporated into a one-dimensional harmonic transport model. The harmonic method utilizes the fact that nearly all of the energy in the system is in a few fundamental tidal frequencies, the first overtides thereof and the mean flow. This allows the representation of the flow as a series of harmonic components whose spatial variability is determined by the model. The model provides a qualitative explantation for and accurate quantitative predictions of along-channel variations in tidal properties in terms of the momentum balance. Near the mouth of the estuary, the boundary shear stress, the pressure gradient and the acceleration terms are all important in the force balance, and the tide behaves like a damped oscillator. Far upriver the pressure gradient is primarily balanced by friction at the bed and tidal wave propagation can be described as a diffusion process. Changes in the channel width in mid-estuary cause partial reflection of the tidal wave and a maximum in tidal range. This partial reflection decreases the tidal energy flux in the upstream direction.

The distribution of the time averaged energy fluxes was also determined from the model. The analysis shows that there are two regions of high energy dissipation. Energy is supplied near the mouth of the estuary by the divergence of the landward flux of tidal potential energy and far upriver by the divergence of the seaward flux of fluvial potential energy. These two regions of high dissipation are separated by a region of low dissipation, the energy flux divergence minimum. This spatial division of the estuary is mirrored in the system biology and geology. It is likely that the energy flux divergence minimum is a common feature of shallow estuaries with strong riverflow.

Introduction

This study focuses on the energetics of the interaction of the barotropic tidal wave, riverflow and topography in shallow estuaries. The work done by tidal and fluvial energy fluxes in such systems causes sediment transport and mixing of river water with heavier ocean water. It indirectly, but strongly, affects biological productivity. Information

0272–7714/89/060549 + 23 $03.00/0

about the spatial and temporal distribution of dissipation and energy flux divergences can therefore provide insight into many aspects of estuarine dynamics. Tidal forcing from the ocean normally provides the dominant source of mechanical energy near the mouth of an estuary. Potential energy is converted to kinetic energy and then dissipated as the tide propagates. In estuaries with fresh water runoff, there is an additional energy source—fluvial potential energy released as the riverflow descends the mean surface gradient. The tidal energy input occurs at well-defined diurnal and semidiurnal frequencies, while most of the energy in the riverflow fluctuations is found at seasonal time scales.

Several different approaches have been used to estimate the dissipation rates and energy fluxes in estuarine energy budgets. These include direct measurement of tidal currents and elevations (Levine & Kenyon, 1975; Bokuniewicz & Gordon, 1980; Brown & Trask, 1980), analytic solutions fitted to boundary conditions (Taylor 1919; Proudman, 1952) and numerical models. Construction of an energy budget from field data is difficult, because the short records usually available from current meters limit the accuracy to which harmonic constants may be determined. Even small uncertainties in these harmonic constants can cause unacceptably large errors in the higher-order terms in the energy budget. Similarly, inadequate representation of topographic complexities may limit the utility of analytical calculations of energy flux. Numerical models are often, therefore, the best way to examine the tidal dynamics of complex systems such as the Columbia River Estuary.

Of the various types of numerical models, we have used the harmonic method as developed by Dronkers (1964), Pearson and Winter (1977) and Snyder *et al.*, (1979). In the harmonic method, tidal heights and currents are assumed to have a periodic dependence. Time is transformed out of the governing equations and the remaining spatial dependence of the flow parameters is determined using a grid. The method provides a conceptual simplicity in that the effects of the different terms in the wave equation can be examined individually. The strength of non-linear interactions associated with the finite amplitude of the tide and the resulting energy transfer to overtides and the residual flow may also be readily evaluated. The predicted tidal harmonic constituents can be directly compared to those calculated from observations. Finally, harmonic decomposition provides a computational efficiency that is unmatched by time-stepping techniques, so that a large variety of tidal and fluvial conditions may be simulated very economically. There are two important restrictions on use of the harmonic method. First, the tidal wave must be only weakly non-linear, i.e. the ratio ε of tidal amplitude to mean depth must be small. Second, most of the dissipation in the system must occur in the channels, where the flow is explicitly represented, not over the tidal flats. This requires that the width of the tidal flats be at most the same order as the channel width. Both of these conditions are met in the Columbia River Estuary, but may not be in some other systems of interest.

Estuarine and fluvial characteristics

The lower Columbia River estuary consists of narrow, sand-bedded channels, typically 0·5 to 3 km wide, separated by broad sand flats (Figure 1). Sand waves with amplitudes between 0·5 and 2·5 m are ubiquitous (Sherwood *et al.*, 1989). The maximum salinity intrusion length varies from 18 to 50 km (about 12–30 river miles). Although tidal effects extend at least 150 km upriver from the entrance to the vicinity of Vancouver, WA, our focus of interest was the lower 80 km of the system, in which tidal forcing is either dominant or of moderate importance in the barotropic dynamics. Modelling of tidal

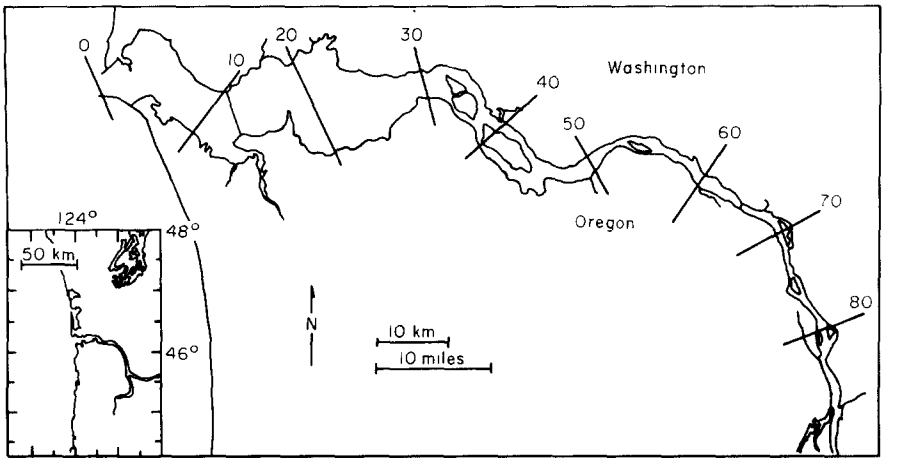

Figure 1. Study location and channel configuration of the Columbia River Estuary. Officially designated River Miles (RM) are shown by bars to facilitate comparison with nautical charts.

propagation required, however, treatment of the entire reach in which tidal effects are observed.

The tide at the mouth of the estuary is of the mixed diurnal and semidiurnal type. The ratio of the semidiurnal to the diurnal constituents varies spatially and seasonally from about 1·5 to 2·1. The major semidiurnal constitutents are M_2, S_2, and N_2 [Table 1 and Figures 2(a) and (b)]. These constituents will be considered in the analysis which follows. The largest semidiurnal neglected is K_2, which is less than 7% as large as M_2. Model results presented below show that M_2 accounts for more than 80% of the total tidal energy flux. Taking the tidal energy flux as quadratic in tidal amplitude, it can be estimated that neglect of K_2 causes errors of about 0·6% in the energy budget. The major diurnal constituents are K_1, O_1 and P_1; K_1 and O_1 were considered in the model. Although K_1 is almost half as large as M_2, it contributes only about 10% of the total tidal energy flux. Moreover, the interaction of O_1 with K_1 was found to be very similar to that of M_2 with S_2 or N_2, and O_1 contributes a very small part (about 4%) of the total tidal energy flux. Thus, all runs presented herein employ only the mean diurnal forcing represented by K_1.

Power spectra of tidal heights [Figures 2(a) and (b)] for two stations in the river-estuary system illustrate several important features of the along-channel evolution of the tide. The spectrum at km(river kilometer)-5 [rivermile or RM-3; Figure 2(a)] shows the energetic dominance of the semidiurnal and the diurnal constituents. Overtides are present in Figure 2(a), but are of such small amplitude that they are energetically unimportant. The spectrum from km-69 (RM-43) shows not only an increase in the importance of the semidiurnal motion relative the diurnal tide [Figure 2(b)], but a much larger increase at overtide (terdiurnal, quarterdiurnal and higher) and tidal monthly frequencies. Both overtides and the residual flow are driven by non-linear interactions associated with finite tidal amplitude. To understand these non-linear effects, we have included the zero-frequency residual and the largest terdiurnal (MK_3) and quarterdiurnal (M_4) constituents in the model.

Along-channel variations in channel cross-section strongly affect the propagation of the tidal wave. Stream width b, total width b_t and mean depth h_o are shown in Figures 3(a)

TABLE 1. Tidal constituent ratios—Columbia River and Estuary

Length of record	km	RM	M_2	$\frac{S_2}{M_2}$	$\frac{N_2}{M_2}$	$\frac{M_4}{M_2}$	$\frac{M_6}{M_2}$	$\frac{K_1}{M_2}$	$\frac{O_1}{M_2}$	$\frac{P_1}{M_2}$	$\frac{MK_3}{M_2}$	$\frac{M_2+S_2+N_2}{O_1+K_1+P_1}$
5 months	1·6	1	0·823	0·273	0·219	0·030	0·002	0·478	0·311	0·148[a]	0·006	1·59
7 months	5·0	3	0·833	0·255	0·207	0·026	0·006	0·487	0·328	0·170	0·015	1·51
7 months	13·3	8·3	0·935	0·256	0·202	0·027	0·006	0·441	0·276	0·132	0·011	1·72
1 year	28·4	17·6	0·947	0·247	0·189	0·012	0·012	0·423	0·252	0·122	0·025	1·81
7 months	39·4	24·4	0·897	0·238	0·185	0·042	0·015	0·400	0·238	0·108	0·036	1·91
1 year	67·7	42·0	0·736	0·234	0·188	0·110	0·013	0·384	0·205	0·107	0·089	2·05
7 months	86·0	53·3	0·578	0·236	0·176	0·155	0·009	0·385	0·200	0·089	0·122	2·10
1 year	134·0	83·0	0·231	0·236	0·195	0·208	0·040	0·478	0·241	0·087	0·145	1·78

[a]Determined by inference

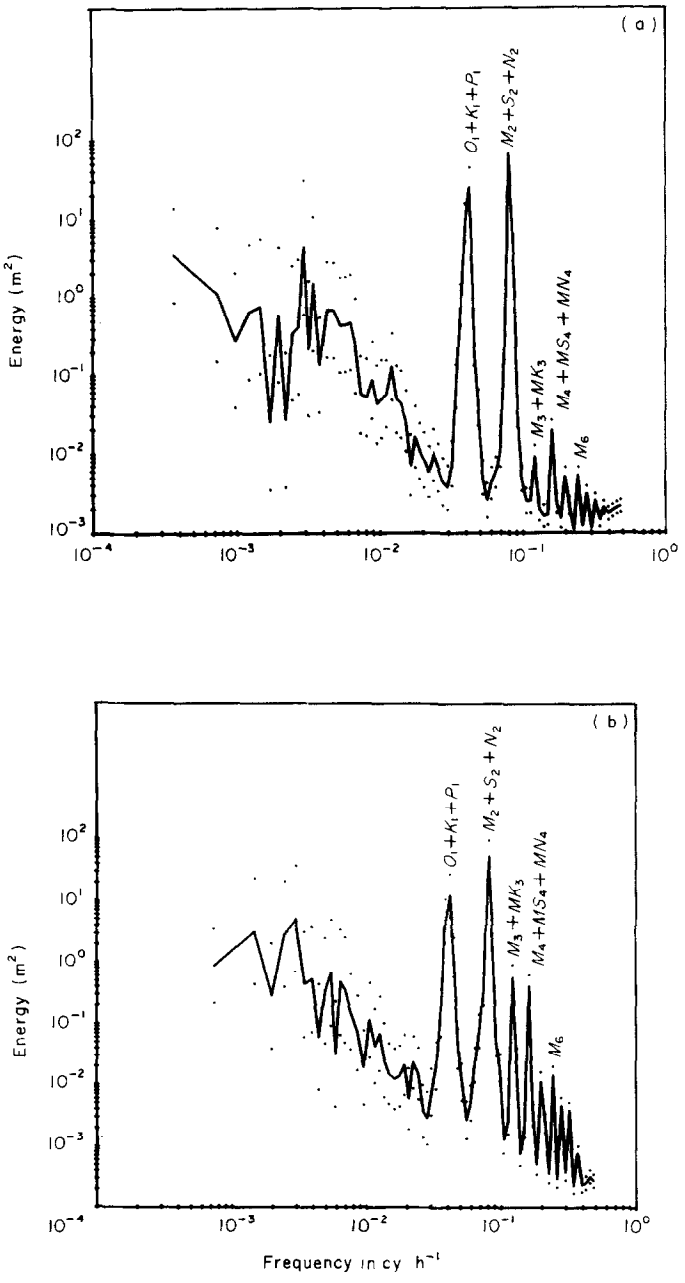

Figure 2. Power spectra at (a) km-5 (RM-3) and (b) km-69 (RM-43); 95% confidence limits are indicated by dots. Overtides and tidal monthly oscillations grow in the upriver direction, at the expense of the diurnal and semidiurnal tides.

and (b). The stream width differs from the total width by the width of the tidal flats b_f. Width b increases and depth h_o decreases with distance upriver for the first 25 km; the resulting cross-sectional area is fairly constant [Figure 3(c)]. There is then a maximum in cross-section associated with wide tidal flats at about km-30. Between km-30 and 60

cross-sectional area decreases sharply from about 50×10^3 to about 18×10^3 m^2. Upriver of km-60 the depth is relatively constant, but the width decreases slowly. Most of the tidal flats are contained in the four peripheral bays in the lower estuary. Their total area is 117 km^2 or nearly 30% of the surface area in the system. While only the flow through the stream width b conveys momentum in the along-channel direction, flats store water and contribute to the tidal prism. Moreover, the flow of water to and from these shallow areas exerts an important non-linear effect on the propagation of the tidal wave along the adjacent channel.

The Columbia River drains $6{\cdot}5 \times 10^5$ km^2 of the Northwest United States and Canada. This drainage is divided into two subsections. The larger portion, the Eastern sub-basin, drains the mountainous interior where most precipitation occurs during the winter. A smaller drainage area, the Coastal sub-basin, includes the west side of the Cascade range. There are usually two peaks in the annual river discharge cycle, one in mid-winter caused by increased rainfall at low elevations in the Coastal sub-basin, and one in spring due to snowmelt in both sub-basins. The total; annual average flow at the mouth is $7{\cdot}5 \times 10^3$ m^{-3} s^{-1} (1000 cubic meters per second), with a maximum monthly average of $10{\cdot}5 \times 10^3$ m^{-3} s^{-1} in June and a minimum monthly average of $4{\cdot}1 \times 10^3$ m^{-3} s^{-1} in September. Flow regulation has strongly altered the natural riverflow cycle over the last two decades, moderating extreme flows, increasing high-frequency flow variations and decreasing sediment transport (Sherwood *et al.*, 1989).

Methods

We have used a one-dimensional harmonic transport model to study the tidal energetics of the Columbia River Estuary. Following Dronkers' (1964) approach, the flux form of the one-dimensional (cross-sectionally) integrated momentum equation is found by replacing the velocity with the transport divided by the cross-sectional area of the stream. Assuming that the estuary is well mixed and that the flow is uniformly distributed throughout the cross-section, the equation of motion is:

$$\frac{1}{hb}\frac{\partial q}{\partial t} - \frac{q}{h^2 b}\frac{\partial h}{\partial t} + \frac{q}{h^2 b^2}\frac{\partial q}{\partial x} - \frac{q^2}{h^3 b^2}\frac{\partial h}{\partial x} + g\left(\frac{\partial h}{\partial x} + S\right) + \frac{c_d}{h^3 b^2} q|q| = 0, \tag{1}$$

where $h(x,t)$ is the axially and time dependent depth, $b(x)$ is the stream width, $q(x,t) = uhb$ is the transport, u is the axial component of the velocity, g is the acceleration due to gravity, S is the slope of the bottom and c_d is a dimensionless friction coefficient. The term gS appears in the equation of motion because the x axis is parallel to a plane of constant gravitational force, not the sloping river bottom from which depths are measured (Figure 4). Equation (1) also excludes the effects of the earth's rotation and the effect of wind stress over the water surface. The time dependent height h' is small compared to the mean depth h_o, so the term $(hb)^{-1} = [(h_o + h')b]^{-1}$ is replaced with $(h_o b)^{-1} = A^{-1}$. The flux form of the continuity equation is:

$$\frac{\partial q}{\partial x} = -(b + b_f)\frac{\partial h}{\partial t}, \tag{2}$$

taking into account flow of water over the tidal flats (Speer & Aubrey, 1985). The second and third terms on the left hand side of equation (1) may be combined by using equation (2). The magnitude of the various terms in the equation of motion may then be determined by assuming $q/A \sim 1$ m s^{-1} and $h' \sim 1$ m:

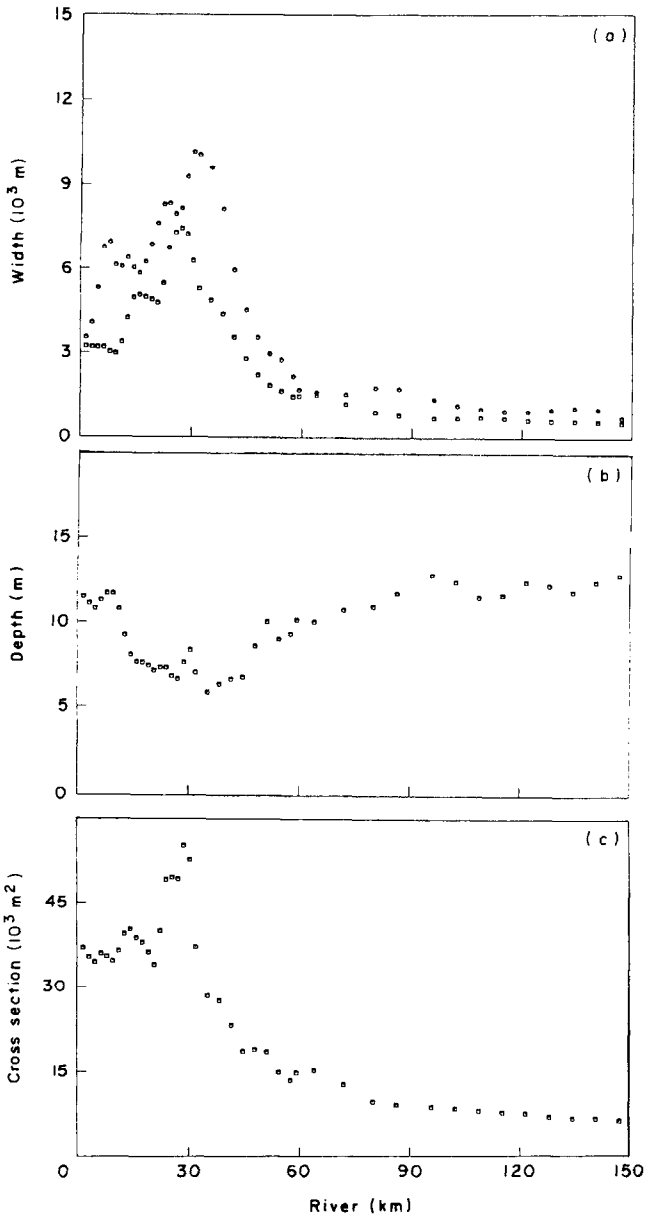

Figure 3. Total width $b+b_f$ (○) and stream width b (□) of the (a) estuary in 10^3 m, (b) depth h_o in m (b) and (c) mean cross-sectional area bh_o in 10^3 m^2 (c). Only the stream width conveys momentum in the model.

$$\frac{1}{A}\frac{\partial q}{\partial t} \sim 10^{-4}\frac{\text{m}}{\text{s}^2} \qquad \textit{Time Dependence (A)}$$

$$\frac{(2b+b_f)}{A^2} q \frac{\partial h}{\partial t} \sim 10^{-4}\frac{\text{m}}{\text{s}^2} \qquad \textit{Advection (B)}$$

$$\frac{q^2}{h^3 b^2}\frac{\partial h}{\partial x} \sim 10^{-6}\frac{\text{m}}{\text{s}^2} \qquad \textit{Advection (C)}$$

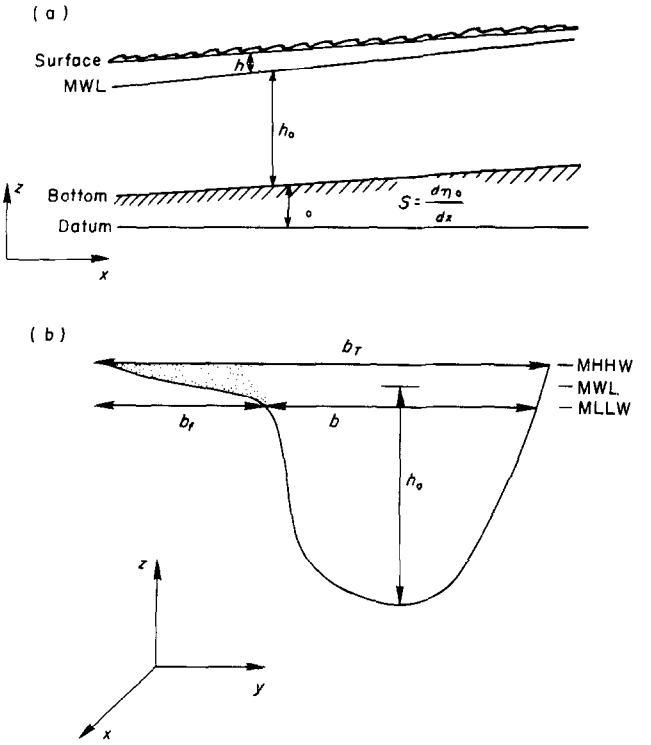

Figure 4. Tidal model geometry; (a) definitions of mean depth h_0 tidal height h', bed slope S and bed elevation η_o, and (b) definitions of stream width b and total width $b - b_f$. MWL is mean water level.

$$g\left(\frac{\partial h}{\partial x} + S\right) \sim 10^{-4}\frac{\text{m}}{\text{s}^2} \qquad \textit{Surface Slope (D)}$$

$$\frac{c_d}{A^2 h_o} q|q| \sim 10^{-4}\frac{\text{m}}{\text{s}^2} \qquad \textit{Friction (E)}$$

The magnitude of (C) is much smaller than that of any of the other terms and was neglected in the model. This does not exclude its possible importance at times when the dominant surface slope and friction terms are small, e.g. at slack water; however, the tidal part of q^2 vanishes at slack water. Note also that the above tidal scaling of the time-dependent momentum equation correctly scales the zero and overtide frequency non-linear terms that drive the residual and overtide circulations. Taking the bilinear $q\frac{\partial h}{\partial t}$ as an example, the dominant contribution comes from h' and the tidal part of q, because the tidal residual contributions to h and q are small for $\varepsilon < 1$.

Neglect of the Coriolis force and wind stress is justified as follows. Near the mouth of the lower estuary the cross-stream velocity is typically $0{\cdot}1\ \text{m s}^{-1}$ or less, so the Coriolis term omitted from equation (1) is small ($fv \sim 10^{-5}\ \text{m s}^{-2}$). Moreover, because the Coriolis force acts normal to the motion, it cannot contribute to the energy budget for the along-channel flow. The average wind stress over the estuary is $3{\cdot}0 \times 10^{-3}\ \text{N m}^{-2}$, so that wind forcing [of $O(10^{-7}\ \text{m s}^{-2})$] is also small in the long-term energy balance. Jay (1987) has

further shown by a statistical and dynamical analysis of residual surface elevations and slopes that atmospheric forcing is less important at sub-tidal frequencies in this system than fluvial and tidal monthly effects. Finally, neglect of the atmospheric forcing is justified, because it is typically greatest at periods of a few days to perhaps 10 days, in the spectral gap between tidal daily and tidal monthly. Thus, it does not overlap in frequency space with any of the major tidal processes.

The equation of motion (1) may then be approximated by:

$$\frac{1}{A}\frac{\partial q}{\partial t} - \frac{(2b + b_f)}{A^2} q\frac{\partial h}{\partial t} + g\left(\frac{\partial h}{\partial x} + S\right) + \frac{c_d}{A^2 h_o} q|q| = 0. \tag{3}$$

The total depth $h(x,t)$ and transport, $q(x,t)$ are assumed to have the sinusoidal form

$$h(x,t) = h_o(x) + \sum_{n=1}^{4} [H_n(x)e^{niwt} + H_{-n}(x)e^{-niwt}] \tag{4a}$$

$$q(x,t) = q_r + q_o(x) + \sum_{n=1}^{4} [Q_n(x)e^{niwt} + Q_{-n}(x)e^{-niwt}]. \tag{4b}$$

Here the terms q_r and q_o are real values for the riverflow and tidally induced mean flow, while the H_n and Q_n are complex functions representing the amplitude and phase of the tidal part of the heights and currents. The limits of the summation represent the four tidal species considered in the model: diurnal, semidiurnal, terdiurnal and quarterdiurnal. The above decomposition also assumes that the dominant diurnal frequency (K_1) is one half of the semidiurnal (M_2) frequency, causing an error of about 10% in the time dependence of the diurnal term.

Using the harmonic decomposition (4) in the equation of motion (3) and continuity (2), the mean or residual flow is specified by

$$\sum_{l,m}\left[g\left(\frac{\partial h_o}{\partial x} + S\right) + \frac{liw(2b + b_f)}{A^2} H_l Q_m + \frac{c_d}{A^2 h_o} P_0\right] = 0, \tag{5a}$$

$$q_0 + \sum_{l,m}\left(\frac{1}{h_0} H_l Q_m\right) = q_r, \tag{5b}$$

where q_r is the riverflow, P_0 is a Chebyshev polynomial representation of the mean bed stress (Dronkers, 1964), and the summation over the integers l,m runs over all combination such that $l+m=0$ and $-4 \leqslant l,m \leqslant 4$. The advantages and accuracy of the Chebyshev polynomials will be discussed below. Non-linearities that drive the residual flow include the convective accelerations and bed stress in equation (5*a*) and the Stokes drift in equation (5*b*).

The nonzero frequencies nw satisfy, with the requirement that $l+m=n$, a wave equation of the form:

$$e^{niwt}\sum_{l,m}\left(g\frac{\partial^2 H_n}{\partial x^2} - \frac{liw(2b + b_f)}{A^2}\frac{\partial}{\partial x}(H_l Q_m) + \frac{niw}{A}\frac{\partial Q_n}{\partial x} + \frac{c_d}{A^2 h_o}\frac{\partial}{\partial x} P_n\right) = 0, \tag{6}$$

where P_n is the Chebyshev polynomial at frequency n. Equation (6) is formed by taking a derivative of equation (3) and using continuity in the form

$$e^{niwt}\left[\frac{\partial Q_n}{\partial x} - \sum_{l,m}\left(\frac{1}{h_0} H_l Q_m\right) = -niw(b + b_f)H_n\right], \tag{7}$$

to eliminate $\partial Q_n/\partial x$. The four equations determined by varying n from 1 to 4 in equation (6) each represent a second order non-linear partial differential equation for the tidal

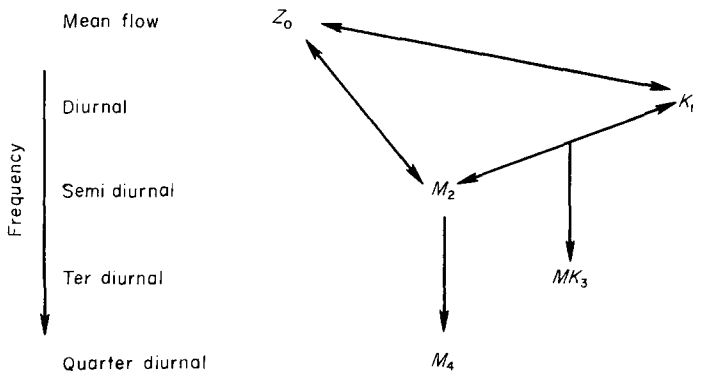

Figure 5. A schematic diagram of non-linear interactions used in the model. Frequency is indicated on the vertical axis. The arrows indicated the direction of energy transfer; a double-headed arrow indicates that energy can flow in either direction.

height constituent H_n. The driving non-linearities for the overtides in equation (6) are the convective accelerations and bed stress. There is another non-linearity in equation (7) which represents overtide generation by wave steepening. This term does not, however, appear for the major diurnal and semidiurnal constituents, for which mass conservation is linear. Thus, for examples, the interaction of K_1 with itself, which in reality generates motion at the frequency of K_2, does not contribute to M_2 in the model.

There are two boundary conditions in this problem, one at the mouth of the river and the other far upstream. The boundary condition at the mouth is that the phase and amplitude of all of the tidal constituents are known. The boundary condition far upstream is that the tidal heights and currents tend toward zero in a uniform manner. The riverflow q_0 is known everywhere and, in the absence of other sources of freshwater, is the discharge at the upstream end.

The solution of this problem requires that the estuary be divided up into sections within which the width and depth vary only slightly. For this study 47 sections were used to model the lower 160 km of the estuary. The grid has variable spacing, sections are 1·6 km long in the first 30 km of the estuary and up to 7 km long further upriver. With such a division the wave in each section can be represented as

$$H_n = C_1 e^{K_1 x} + C_2 e^{K_2 x} \tag{8a}$$

$$Q_n = -niw(b + b_j)\left(\frac{C_1}{K_1} e^{K_1 x} + \frac{C_2}{K_2} e^{K_2 x}\right) \tag{8b}$$

$$K_j = ik_j + r \qquad j = 1,2 \tag{8c}$$

where the wavenumber K_1 represents the incident, landward propagating wave and K_2 represents the reflected wave. Each K_j is a complex number of which the real part (r) represents damping and the imaginary part (ik_j) represents wave propagation. The difference in wave speed between the incident and reflected waves arises from the fact that the former must propagate against the riverflow, while the latter propagates with the riverflow.

The difficulty in solving equations (5*a*,*b*) and (6) stems from the presence of the non-linear interaction terms. In each non-linear term, two or more time-dependent quantities are multiplied together resulting in the generation of terms which have frequencies that

are the sums and differences of the initial frequencies. Constituents subscripted l and m are present in equations (5*a*,*b*) and (6) for frequency n, where $l,m \neq n$. Interactions between the mean, the diurnal and the semidiurnal currents act to transfer tidal energy to both higher (overtide) and sub-tidal (residual) frequencies. The overtides grow in the upstream direction relative to the forcing frequencies, reflecting the distortion of the wave. The magnitude and phase of these non-linearly forced motions are important to the dynamics of the estuary and in the absence of riverflow may determine whether the estuary is flood or ebb dominant (Aubrey & Speer, 1985). The Columbia River Estuary is always ebb dominant however, because of the strong riverflow.

Not all of the interactions between the semidiurnal and diurnal tides and the smaller overtides were included, because most of the energy in the system is in the riverflow and semidiurnal and diurnal tides, not the overtides. The sources of non-linear interactions are shown schematically in Figure 5. A double headed arrow represents an interaction in which energy is transferred in both directions. A single headed arrow indicates a uni-directional energy transfer from one frequency to another. For example, the self-interaction of the M_2 tide generates both a zero-frequency residual flow and the M_4 tide. The mean flow-M_2 interaction is, because of the strong riverflow, important everywhere, is included in the model, and accounts for the double-headed arrow between M_2 and the mean flow. In contrast, the M_4-M_2 interaction does not significantly affect the M_2 tide except far upriver. Thus, only energy transfer from M_2 to M_4 has been included in the model, accounting for the single arrow between M_2 and M_4. Neglect of the feedback of the overtides onto the driving tidal frequencies is justified even far upriver, however, because the energy budget of this portion of the system is dominated by riverflow.

The absolute value in the bed friction term $c_d|q|q$ causes it always to oppose the flow, changing sign when the velocity changes direction. Solution of the wave equation requires that $|q|q$ be represented by some other function so that the sign of the friction term can be found as a function of time. An accurate method of approximating $|q|q$ while retaining its non-linear nature is to replace the absolute value with a polynomial and resort to an iterative solution for the non-linear terms. The third-order Chebyshev polynomial defined by Dronkers (1964) has been employed for this purpose:

$$q|q| = \frac{c_d}{\pi} U^2 b^2 h_o^2 (d_0 + d_1\hat{q} + d_2\hat{q}^2 + d_3\hat{q}^3) \tag{10}$$

Where U is the velocity scale and carats indicate non-dimensional variables. The coefficients d are functions of the ratio of riverflow to tidal flow. The coefficient d_0 does not appear in the wave equation (6), because of the differentiation necessary to obtain equation (6) from (3). In the mean flow equation, equation (5*a*) d_0 has been neglected, because it is never more than 7% of the largest of the d_i and is typically less than this.

The advantages of this representation include the harmonic nature of the functions employed, an ability to account for the increased duration of the ebb associated with the presence of riverflow, and minimization of error near maxima (Carnehan *et al.*, 1969). Correct representation of maxima is important because the quadratic nature of the friction term enhances its importance at the extreme values of velocity; this is even more important in estimation of the dissipation. The resulting fit of the Chebyshev polynomial to the function $q|q|$ is generally good (Figure 6). The fit is least satisfactory in the vicinity of the zero crossing, but the position of the zero crossing itself is accurately determined, so that the sign of the stress is correct. The polynomial representation is most accurate in the lower estuary, where the ebb and flood currents are approximately equal, and far upriver,

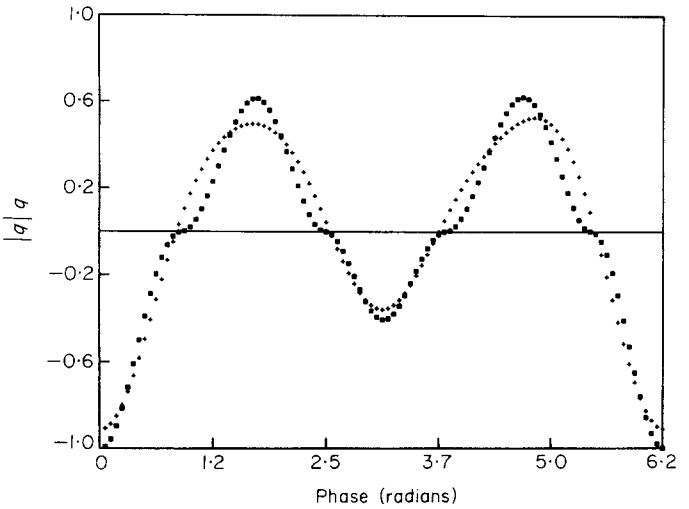

Figure 6. The fit of the Chebyshev polynomials to the curve $q|q|$. The actual curve is shown by (■) and the approximation is indicated by the (+).

where the tidal flow is small relative to the fluvial flow. It incurs a greater error in the intermediate regime in which tidal and fluvial currents are of comparable strength and the ebb-flood asymmetry is substantial. This is, however, the part of the estuary with the weakest friction and dissipation (below).

The strength of the coupling of the flow to the bed is parameterized by the drag coefficient c_d; $c_d = 0{\cdot}003$ was used throughout the system upstream of salinity intrusion. Where salinity intrusion is present, the shear stress at the bed is reduced by stratification in the water column, partially decoupling the overlying flow from the bottom. An empirical value of $c_d = 0{\cdot}0008$ was used seaward of km-20 (RM-12) (the average salinity intrusion length) to compensate for this effect. Reduction of c_d in the lower estuary was also useful in a two dimensional, vertically integrated finite difference model (P. Hamilton, personal communication). These values of c_d are, moreover, comparable to those calculated for a highly stratified flow in the Fraser River Estuary (Geyer, 1985). Geyer obtained two different estimates of c_d. One, based on dune roughness (the dunes being 0·4 to 0·7 m in height), was 2·6 to $3{\cdot}0 \times 10^{-3}$. It is appropriate to a neutrally stratified flow and agrees well with that used in our model upstream of salinity intrusion, although the dunes in the Columbia River Estuary are somewhat larger than those in the Fraser River Estuary. The second estimate, $c_d = 1{\cdot}0$ to $1{\cdot}6 \times 10^{-3}$, was derived from the observed vertical distribution of the along-channel tidal flow, and is close to the value used in our model for the stratified part of the system. Geyer also attributes the difference between the two estimates to the reduction in drag caused by stratification.

The solution to the second order, non-linear wave equation (6) is found iteratively using a Gaussian-elimination technique as discussed by Dronkers (1964) and Pearson and Winter (1977). An initial estimate of the tidal current for the largest tidal constituent (M_2) is made for each section of the estuary, so that the friction terms can be specified. With this estimate, equation (6) is solved by imposing the upstream boundary condition and then matching solutions at the boundaries of each section. At the mouth of the estuary the other boundary condition is imposed and then the heights and currents of the M_2 tide are found for the entire estuary. Using this solution for the semidiurnal tide,

the diurnal tide is calculated next and then the overtides. This process is repeated until all of the tidal constituents relax to a solution which does not vary by more than 1% from iteration to iteration. The diurnal and semidiurnal constituents relaxed quickly, usually within ten iterations. The non-linearly forced overtides were more sensitive and required as many as 25 iterations.

The energy equation is found by multiplying the momentum equation (1) by pu and then averaging over a tidal cycle (Bokuniewicz & Gordon, 1980):

$$\frac{q}{A}\left\{\frac{\partial}{\partial x}\left(\rho g h + \frac{1}{2}\frac{\rho g^2}{A^2}\right)\right\} = \frac{\rho c_d}{A^3 h_o} q^2 |q|. \tag{11}$$

where an overbar indicates a tidal cycle average. The left hand side of this equation represents the divergence of total energy flux (kinetic plus potential) through a section. The right hand side represents the energy loss due to frictional dissipation; the energy flux divergence is exactly balanced by dissipation. Direct gravitational attraction between the moon and the estuary can also contribute to the energy balance in a manner neglected in equation (11). When the moon passes over the main body of the estuary it exerts a gravitational attraction on the water. The work done by the moon can be either of positive sign in which case the estuary gains energy, or negative in which case the estuary loses energy to the moon. Using average values for all of the above variables, the average work done by the moon is only 2–4% of the other terms and has been neglected herein.

Model results and discussion

The model was run for varying tidal forcing and riverflow conditions. The spectrum of possible cases runs from neap tides and low riverflow to spring tides and high riverflow. Comparison of predicted M_2 heights and transports with harmonic analysis (Jay, 1984) of observations taken during months with average riverflow (7·5 kcms; Figure 7(a) and (b)) was used as the primary check on model accuracy. M_2 tidal transport amplitudes were estimated using cross-sectional areas and harmonic analysis results from ten current meter moorings. Where there was more than one current meter at the station, the width-weighted M_2 tidal currents were averaged to approximate the transport across the section. Predicted and observed M_2 current amplitudes agree everywhere within 10% and height amplitudes agree within 5% seaward of km-90. Greater height amplitude errors are found at the most landward station, for reasons discussed below.

A conspicuous feature of both observations and model predictions is the amplification of the M_2 tide in the lower estuary [Figure 7(a)]. M_2 tidal amplitudes increase from the entrance to a maximum at about km-30 (RM-18). Model results suggest two factors necessary to produce this amplification. The first, discussed below, is the change in admittance caused by the abrupt decrease in channel cross-section at km-30. Upstream of this constriction the wave is affected by friction and decreases sharply in amplitude. The second is reduced bed stress associated with stratification in the lower estuary. If c_d is not reduced substantially from the usual value of 0·003 in the lower estuary where salinity intrusion occurs, then the along-channel increase in M_2 amplitude in this reach is completely eliminated. The likely reason that the model does not damp M_2 height amplitude rapidly enough landward of km-100 [Figure 7(a)] is that the representation of the friction (Figure 5) does not include effects of the terms higher in frequency than M_4 and the feedback of these overtides on M_2. As the overtides grow relative to M_2, their influence on

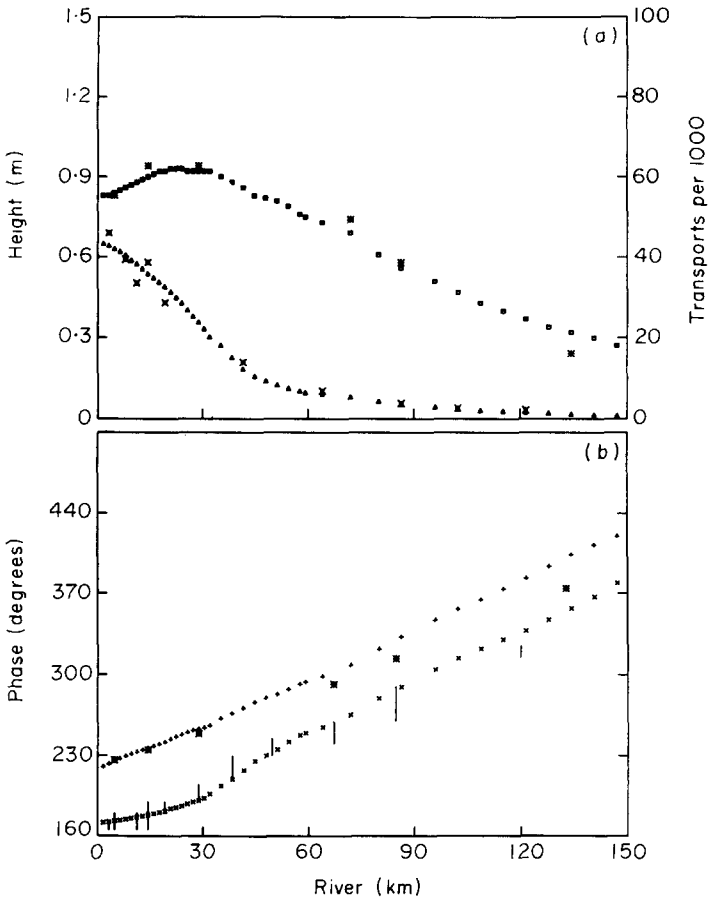

Figure 7. M_2 height (■) and transport (▲) amplitudes (a), and height (+) and transport (×) phase predicted by the model during average riverflow (7500 cm). Measured tidal height properties are shown by six-point stars in (a) and (b) and transport amplitude calculated from current meters in (a). Because of the variability with depth of the transport phase in (b), the observed range of variation of the current phase is shown as a bar.

the bed friction grows quadratically, and the omission of this feedback mechanism becomes important. However, the energy budget in this region is dominated by riverflow, so the energy budget can still be accurately determined.

The observed M_2 tidal height phase increases in a nearly linear manner from the mouth upstream [Figure 7(b), asterisks]. The model accurately predicts (within 12°) the phases in the lower 60 km, however there is a systematic error, which increases upriver. A similar error appears far upriver in the predicted transport phase. These phase errors apparently result from the fact that the model does not include the finite amplitude effect on wave propagation speed. Jay (1989) has shown that the classical result found in Section 187 of Lamb (1932) that $c \sim (gh)^{1/2}[1+(3\varepsilon)/2]$ for an inviscid finite amplitude wave still applies approximately in the presence of friction. This correction is of the correct sign and magnitude to account for the phase errors in Figure 7(b).

Predicted tidal transports decrease very quickly from the mouth, with the sharpest decrease in the lower estuary [Figure 7(a)]. The model shows that this sharp decrease in

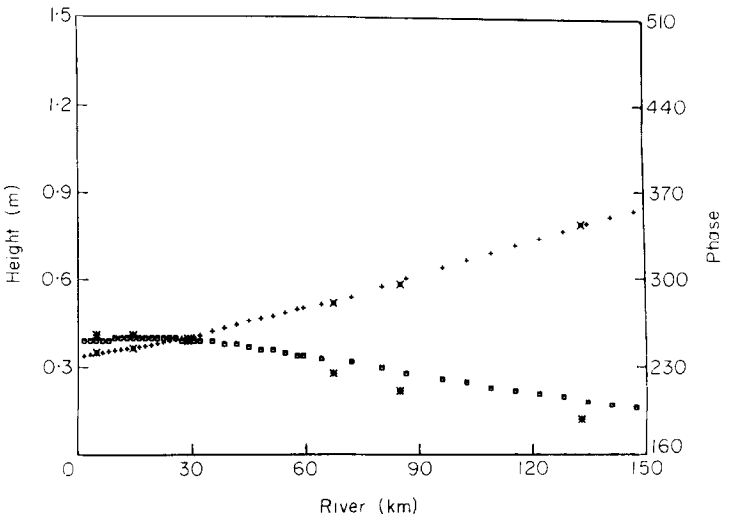

Figure 8. K_1 (a) height, (b) transport for mean riverflow. Symbols for observations are as in Figure 7a. Current meter time series were not long enough to determine K_1 transport harmonic constants from observations.

tidal transport is caused by the presence of extensive tidal flats seaward of km-40 (RM-24), where b_t/b is typically in the range of 1·3 to 2. Landward of km-40 transports decrease more slowly, because tidal flats are less extensive. The cross-sectional variability of the observed current phase is, like the stratification, a feature that cannot be predicted by a barotropic model. The range of this variability [Figure 7(b)] reflects first, channel curvature and other topographic effects, and second, variability of the coupling of the flow to the seabed. This enhances the vertical phase variability in the lower estuary where stratification increases the shear (Jay & Smith, 1988). There is also less progression of the tidal current phases in the lower estuary than upstream because of the partial reflection of the tidal wave found below km-40 [Figure 7(b)]. The greatest phase difference between height and current phases is coincident with the maximum in tidal range and is also associated with this reflection, as discussed below.

The propagation of K_1 through the river-estuary system is rather different from that of M_2 [Figure 8(a),(b)]. The K_1 height amplitude is almost half that of M_2 at the mouth but does not show the same amplification [Figure 8(a)]; it is nearly constant in the lower estuary and then dies off linearly after km-30. The likely reason for this behaviour is, as we will show later, that the effective change in admittance for a diurnal constituent like K_1 is lower than that for a semidiurnal like M_2. Because large changes in admittance give rise to large reflections, the reflection of the diurnal wave is less than that for the semidiurnal tide. Agreement between observed and computed height amplitude is comparable in the case of K_1 to that of M_2; divergence between observations and predictions occurs only above km-60 (RM-37). Agreement between the model prediction of K_1 phase and harmonic analysis results is better than that for M_2 beyond km-45 (RM-28). This is probably because the height amplitude of K_1 is only about 0·4 to 0·5 that of M_2 so that the finite amplitude effect is only $\sim 1/3$ as large. The overestimation of K_1 amplitude landward of km-60 is probably the result of neglect of the frictional feedback of the MK_3, the largest overtide landward of about km-60; Figure 2(b). It does not stem from neglect of the interaction of M_2 with K_1, which is included in the model.

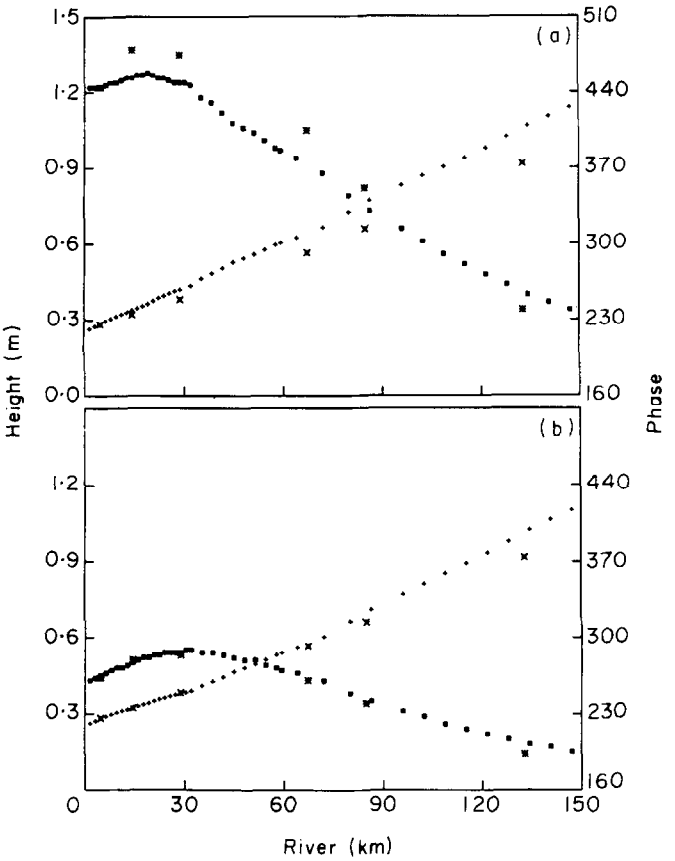

Figure 9. a–b.

Figure 9. Predicted behaviour of (a) $M_2+S_2+N_2$ (the spring tide) and (b) $M_2-S_2-N_2$ (the neap tide), for average riverflow, and (c) of M_2 for low riverflow (4100 cms) and (d) high riverflow (10 500 cms). Symbols for obervations are as in Figure 7a.

Tidal monthly variability of the semidiurnal tidal response was calculated using combinations of tidal constituents, i.e. by treating the semidiurnal species as a whole. Formally, a spring tide occurs when the sun and the moon act together, i.e. when S_2 is in phase with M_2. A tide of even larger range occurs when additional semidiurnal constituents are in phase with M_2. A neap tide occurs when the sun and moon are in opposition. We shall refer informally to any condition of strong semidiurnal forcing as a spring tide and any condition of weak semidiurnal forcing as a neap tide. A spring tide in the model was represented by forcing the model at the boundary with the observed value of $M_2+S_2+N_2$ [Figure 9(a)], and a neap tide by $M_2-S_2-N_2$ [Figure 9(b)]. The tidal wave on spring tide is reduced by strong boundary shear stress, which increases as the square of the amplitude. The decrease in tidal height amplitude landward of the maximum at about km-30 (RM-18) is sharp; by km-35 dissipation has reduced the tidal height amplitude to its initial value at the mouth of the estuary. The tidal transport is reduced to 10% of its value at the mouth by km-60. On neap tide, it is not until km-75 (RM-47) that the tidal height amplitude is reduced to its initial value at the mouth and not until km-80 (RM-50) that the tidal transport decreases to 10% of its original value. The

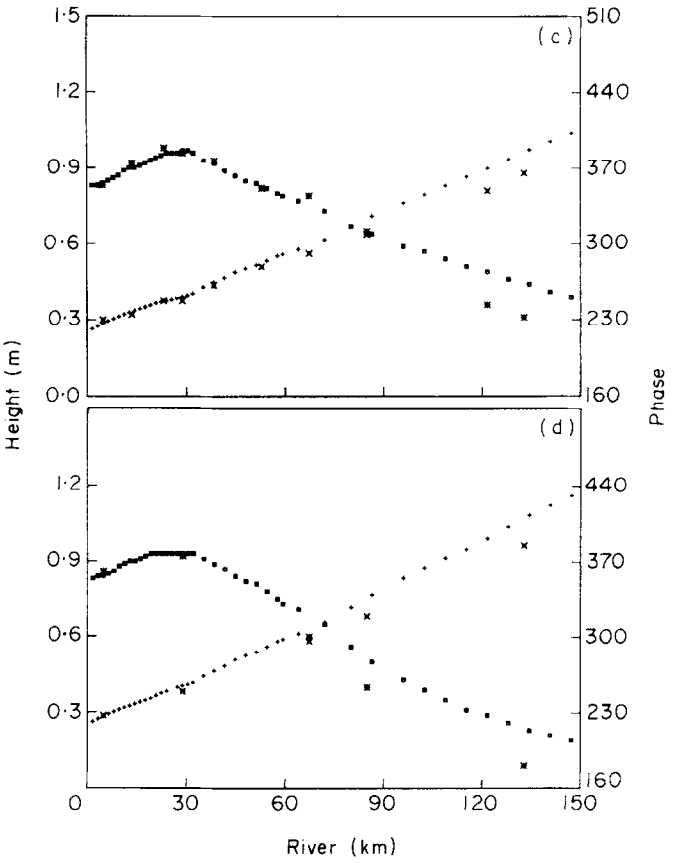

Figure 9. c–d.

stronger non-linearity in the spring tide case causes greatly increased dissipation and also acts to transfer a greater proportion of energy from the astronomical forcing frequencies to both higher and lower frequencies. The semidiurnal tide is therefore more quickly damped on spring tides than during the weakly non-linear neap tides. The growth of the model overtides is correspondingly much more rapid on spring tides. Note that each of the overtides in the model (M_4 and MK_3) represent an entire species and are, therefore, the sum of several overtides. Thus, for example, M_4 in the model is actually $M_4 + MS_4 + MN_4$. The phase relationships among these constituents vary over the tidal month, accounting for the predicted variability of M_4. The greater accuracy of the neap tide model predictions relative to those for spring tide is consistent with earlier arguments concerning the sources of error in the model. That is, both overtide friction and finite amplitude effects (and the errors caused thereby) are greater on tides of large range.

The model was also used to examine the effects of riverflow on tidal characteristics. Runoff acts in a non-linear manner through advection by the mean flow and through the higher-order friction terms. It is not important in the lower estuary where cross sectional areas are large but becomes important upriver where the tides are weak and riverflow is strong. The M_2 tidal response is shown in Figures 9(c) and 9(d) for low and high riverflow. High riverflow strongly suppresses tidal heights above km-60 (RM-37). For example, at

km-100 (RM-62) the M_2 tidal amplitude is about 0·6 m in the low-flow case, whereas it is only 0·4 m in the high-flow case. A similar reduction in tidal heights is apparent in the data, but both model runs overestimate tidal amplitudes far upriver. The tidal wave propagates more slowly during high riverflow periods for two reasons. First, friction is increased by the runoff, increasing the wavenumber for both waves. Second, the adverse riverflow increases the speed discrepancy between the incident and reflected waves. Because the reflected wave is small landward of km-60, this also slows wave propagation.

One of the reviewers brought to our attention an analysis of frictional effects on tides in shallow river estuaries by Parker (1984). While his treatment of the bed stress is based on a Fourier expansion rather than Chebyshev polynomials, Parker's analysis also shows strong frictional suppression by riverflow of the M_2 tide in a convergent estuary (the Delaware). Parker further emphasizes the role of the frictional non-linearities in generating odd overtides (e.g. M_6). We did not calculate M_6, because it is quite small relative to M_4 at upriver stations, where non-linear generation mechanisms are important. However, equation (10) suggests two frictional generation mechanisms for M_6: the cubic interaction of M_2 with itself (proportional to d_3), and the interaction of M_2 and M_4 (proportional to d_2). Since d_2 increases and d_3 decreases with riverflow, it is likely that the latter mechanism is more important in the upriver portions of the Columbia River Estuary.

The sensitivity of the system response to changes in riverflow and tidal range suggests that variability in these forcing functions will impose temporal changes on the energy budget of the estuary, but on different time scales. The astronomical tidal forcing has a strong fortnightly time dependence, while the runoff varies seasonally. To understand the energy distribution, however, we must further consider the spatial and temporal structure of the tide wave itself.

One of the most important characteristics of the tide is the phase difference δ between tidal heights and tidal currents. In a standing wave δ is 90°, while in a pure progressive wave δ is 0°. A standing wave can be thought of as the sum of two pure progressive waves, one directed landward and one of equal amplitude directed seaward. The landward energy flux associated with the incident wave is in this case exactly balanced by the seaward energy flux of the reflected wave; there is no net energy flux. In dissipative situations the reflected wave will be frictionally attenuated and must be smaller in amplitude than the inbound wave except at a point where total reflection occurs; a perfect standing wave is impossible. When friction becomes so important that the effects of acceleration are negligible in the wave equation, the force balance is between the pressure gradient and the bed stress. LeBlond (1978) has termed this the frictionally diffusive regime. The real and imaginary parts of the wave number are equal, and δ for such a wave is, in the absence of a reflected wave, 45°. This same force balance also occurs when the effects of moderate channel convergence and acceleration balance each other in the wave equation. Thus, values of δ between 0 and 90° may be achieved either by partial reflection or through the effects of strong friction and convergence.

The effects of friction and reflection on wave behaviour can be further understood by considering the impedance or its inverse, the admittance, Y. Y is the ratio of system response to system forcing (or $\frac{q}{h'}$ for a constant density flow; Lighthill, 1978). Reflection of a wave occurs only where Y for that wave changes. Application of mass conservation shows that Y for a tidal long wave is proportional to $c(1-ir/k)/(1+r^2/k^2)b_t$, where c is the wave speed and the ratio r/k is an indicator of the strength of friction. The magnitude of Y thus depends directly on the total width b_t and the square root of the depth, while the phase

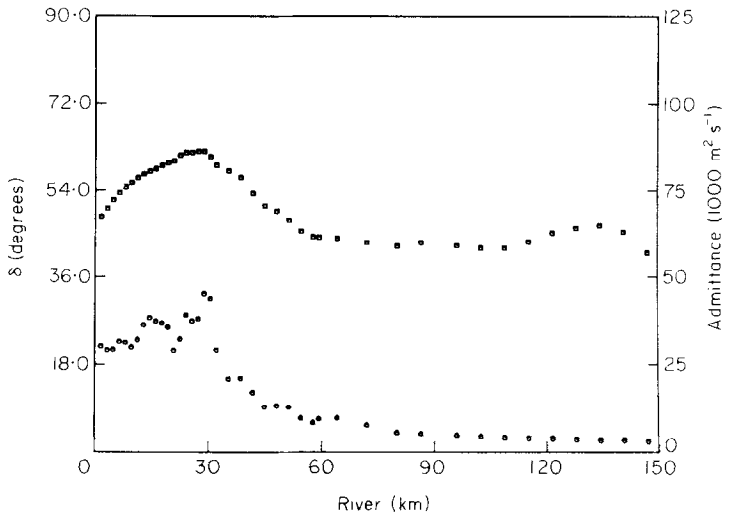

Figure 10. Predicted M_2 admittance Y amplitude and (●) phase difference δ (■) for average riverflow. The maximum in Y and δ nearly coincide with the maximum in height amplitude in Figure 7a. Both are associated with tidal wave reflection off the sharp decrease in width [Figure 3(a)] near km-30 (RM-18).

difference between q and h' for the incident wave depends on the strength of the friction. If the channel ends abruptly Y goes to zero and a reflected wave is emitted in phase with the incident wave. If the channel exits into a much wider bay the effective Y goes to zero and a reflected wave is emitted with a phase change of 180° with respect to the incident wave. Because the total width appears in the equation for Y, the importance of the storage areas becomes clear. In many estuaries the storage widths are as large or larger than the stream widths, and changes in storage width may dominate changes in Y, if, as is the case in the Columbia River Estuary, b_t is more variable than h. Note also that an increase in the strength of friction should increase the phase difference between q and h' by increasing r/k.

The phase difference δ for incident plus reflected wave and the amplitude of the Y for the M_2 tide are plotted in Figure 10; the latter follows closely b_t [Figure 2(a)], while the phase of Y (not shown) is nearly independent of x. The greatest change in Y and, therefore, the greatest reflection both occur at about km-28 (RM-18). In the lower estuary δ increases from about 48° at the entrance to a maximum of 62° at about km-28, indicating that the wave is partially reflected at this point. Further upstream δ tends toward 45°, indicative of a frictionally diffusive region. Because the change in Y is caused largely by a decrease in the stream width, the reflected wave is in phase with the incident wave and the reflection point acts as an antinode. Thus, the amplification of the tide wave and the associated maximum in δ in the lower estuary can be explained in terms of changes in Y of the tidal wave. That K_1 is amplified less in the lower estuary can also be understood in terms of changes in Y. In the strongly frictional regime where acceleration is much weaker than the bed stress, c varies with the square root of frequency. Changes in Y for K_1 should, therefore, be only about $2^{1/2}$ as large for as those for K_1.

The energy flux terms on the left hand side of (11) can also be related to the reflection and transmission of the tidal wave as it propagates through the system. The energy equation (11) contains three terms. The first is the divergence of the potential energy flux

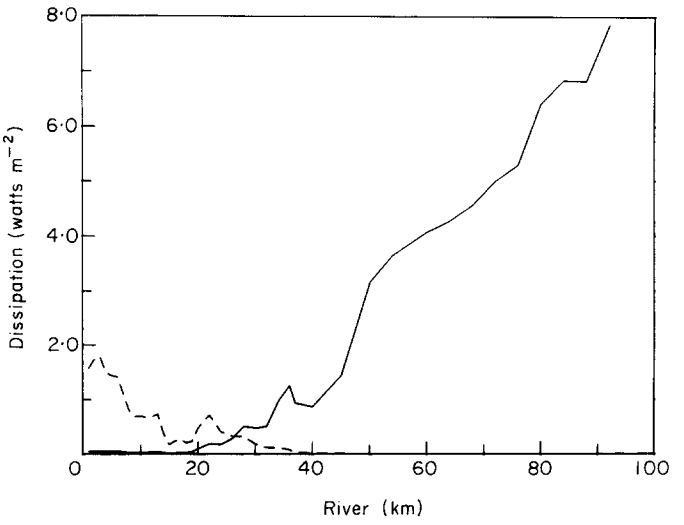

Figure 11. The tidal (– – –) and fluvial (——) dissipation in watts per square meter as a function of along-channel distance for high runoff (10 500 cms) and spring tides ($M_2+S_2+N_2$). The energy flux divergence (EFD) minimum is associated with the partial reflection of the tidal wave at the decrease in width at about km-30.

per unit area $\frac{\rho g}{A}\overline{qh}$, of which the tidal part is $\rho g U_i H_i \cos\delta$ for the i^{th} constituent. In a progressive wave δ is zero and the potential energy flux per unit area is at a maximum; all the energy passing through a cross-section will either be transmitted or dissipated. In a standing wave (without friction) δ is $\frac{\pi}{2}$ and the tidal potential energy flux is zero; all the incident energy is reflected back out of the system. In the fluvial part of the system upstream of about km-60 (RM-37), the fluvial potential energy flux and flux divergence are much larger than the corresponding tidal terms. The second term on the left in equation (11) is the divergence of the kinetic energy flux. The purely tidal part of this vanishes identically, and the remaining tidal-fluvial interaction and fluvial kinetic energy terms are small relative to the tidal and fluvial potential energy terms. The final term on the right is the dissipation; it must closely balance the potential energy flux divergence, so long as the kinetic energy flux divergence terms are small.

The total energy flux divergence (which is equal to the dissipation) is plotted for a spring tide and high riverflow as a function of distance upstream in Figure 11. The high-riverflow, spring tide case is chosen for discussion here, because periods of high velocities and high dissipation are of greatest interest with regard to transporting sediment and governing the form of the channel. It is is possible to break the estuary up into three distinct regions based on the dissipation rates indicated in Figure 11. Upstream of about km-75 (RM-47) the fluvial potential energy flux divergence and the fluvial dissipation are large due to the high runoff velocities associated with the small cross-sectional area. At the month of the estuary (below km-15; RM-9) there is an area of strong dissipation caused by the strong tidal forcing. The primary energy balance is then between the flux divergence of tidal potential energy and dissipation. Between these two highly dissipative sections is a broad region of low energy flux divergence, which we have called the energy flux divergence (EFD) minimum. The EFD minimum occurs where δ is at a maximum, and

the tide most closely resembles a standing wave. Both tidal and fluvial energy fluxes are important in this reach. Downstream of the EFD minimum, the potential energy flux is primarily tidal and is directed upstream, because the incoming tidal wave is larger than the reflected wave. Upstream of the EFD minimum, the potential energy flux is primarily fluvial and is directed downstream because of the mean surface slope of the river. The upstream limit of salinity intrusion is located near the seaward end of the ETM and a maximum in sand deposition is found near its upstream end. System biology is also consistent with the division of the estuary into these three sections (Jay *et al.*, 1988).

The EFD minimum discussed here is related to a local maximum in cross-section and can occur even in the presence of generally strong friction. It should not be confused with a similar phenomenon mentioned by Prandle and Rahman (1980), which occurs at the first current node in weakly frictional systems. This current node can only occur in system more than one-quarter wavelength long and is not related to riverflow.

Conclusions

A one-dimensional harmonic model was used to examine the tidal characteristics of the Columbia River and Estuary, a shallow system with strong tidal forcing and riverflow, a moderate ratio of tidal amplitude to mean depth, and large peripheral storage areas. These characteristics are common amongst coastal plain estuaries. Because of along-channel changes in channel cross-section and the finite amplitude non-linearity of the equations of motion, residual and overtide generation was included in the model, and an iterative solution technique was required. The resulting one-dimensional harmonic method included the riverflow, the tidal residual, and one diurnal, three semidiurnal, and two overtide tidal constituents. It was quite useful in analysis of overtide generation and tidal-fluvial interaction. The computational efficiency of the harmonic method allowed investigation of a wide variety of tidal and runoff conditions.

The model suggests that two factors are responsible for producing the observed amplification of the semidiurnal tide in the lower estuary, up to about km-30 (RM-18). The first is reflection of the semidiurnal wave off of the sharply convergent geometry near km-30. This reflection also acts to increase the phase difference δ between surface elevation and transport. The second is that stratification caused by salinity intrusion into the seaward 20 to 30 km of the system decreases the boundary shear stress in this reach. This reduction in bed friction is reproduced in the model by decreasing the drag coefficient c_d to 0·0008 for the seaward 20 km of the system; c_d was 0·003 otherwise.

The model is more successful in predicting tidal properties near the entrance than far upstream (above about km-100 or RM-62). It is also more accurate for periods of weak to moderate tidal forcing and riverflow than for periods of intense riverflow and extreme tidal forcing. There appear to be two reasons for these failings of the model. First, the model neglects the finite amplitude increase in wave propagation speed. Thus, the phase propagation speed is somewhat underestimated, the cumulative effect of which is most evident far upriver. The second is the omission of the overtide frictional feedback onto the diurnal and semidiurnal tidal constituents. As a result, the amplitude of the major tidal constituents is slightly overestimated upriver, where the overtides are at a maximum. The primary regions of interest in this study were, however, the entrance area and the EFD minimum reach below about km-60 (RM-37), where tidal forcing is at least moderately important. Fluvial effects also grow rapidly above about km-60, and tidal currents are small relative to the riverflow. Minor inaccuracies in the representation of the tidal

processes in this fluvially-dominated reach, therefore, do not detract from the overall utility of the model.

There is a minimum in the time-averaged energy flux divergence (or equivalently, in the dissipation) in the Columbia River Estuary between km-15 and 40 (RM-9 and 25). The EFD minimum is coincident with the widest portion of the estuary where there are large storage basins. It arises because of a narrowing of the estuary at about km-30 (RM-18) and the resulting decrease in admittance. The change in admittance causes reflection of part of the incident tidal potential energy and a local maximum in tidal amplitude. This lessens the amount of tidal energy available to be dissipated landward of this point. Just landward of the EFD (upriver of km-40), damping by the riverflow cause the semidiurnal and diurnal waves to diminish rapidly. A combination of friction and covergent geometry bring about a phase difference between the tidal height and transport for the M_2 tide of about $\frac{\pi}{4}$ above km-60 (RM-37). Fluvial forcing dominates the energy and momentum balances in this part of the system.

The presence of the EFD minimum suggests the division of Columbia River Estuary into three reaches, each characterized by a different energy budget. In the lower estuary the energy budget is dominated by the divergence of the landward flux of tidal potential energy and tidal dissipation. The energy budget shows, therefore, strong tidal monthly variability. Far upriver, the energy budget is dominated by the seaward flux of fluvial potential energy and fluvial dissipation and exhibits strong seasonal variability. Between these two highly dissipative regions lies the EFD minimum region. The net upstream flux of tidal potential energy and the downstream flux of fluvial potential energy are of comparable importance in this reach, but both are relatively small.

It is likely that the EFD minimum is a common feature of shallow, coastal plain estuaries. While the EFD minimum in the Columbia River Estuary results from the interaction of tidal and fluvial forcing, an EFD minimum could also be created by the tidal flow alone in a system with a narrow entrance, a wide bay, and a narrow, convergent channel landward of the bay. This is essentially the inverse of the situation in the Gironde Estuary, where a constriction causes a local maximum in dissipation (Allen *et al.*, 1980).

Acknowledgements

This research was supported by NSF Grant OCE-8208856. Lin Sylwester assisted in preparation of the figures. We thank D. Prandle of Bidston Observatory and David Aubrey of Woods Hole Oceanographic Institute for helpful reviews.

References

Allen, B. P., Solomon, J. C., Du Penhoat, Y., & De Grandpré, C. 1980 Effects of tides on mixing and suspended sediment transport in macrotidal estuaries. *Sedimentary Geology* **26,** 69–80.

Aubrey, D. G. & Speer, P. E. 1985 A study of non-linear tidal propagation in shallow inlet/estuarine systems. Part I: Observations. *Estuarine, Coastal and Shelf Science* **21,** 185–206.

Bokuniewicz, H. J., & Gordon, R. B. 1980 Storm and tidal energy in Long Island Sound In *Estuarine Physics and Chemistry: Studies in Long Island Sound; Advances in Geophysics* (Saltzman, B. ed.). New York: Academic Press, **22,** 41–68.

Brown, W. S. & Trask, R. P. 1980 A study of tidal energy dissipation and bottom stress in an estuary. *Journal of Physical Oceanography* **10,** 1742–1754.

Carnehan, B., Luther, H. A. & Wilkes, J. D. 1969 *Applied Numerical Methods*. New York: J. Wiley, pp. 604.

Dronkers, J. J. 1964 *Tidal Computations in Rivers and Coastal Waters.* Amsterdam: North-Holland Publishing Company, pp. 516.
Geyer, W. R. 1985 The time dependent dynamics of a salt wedge, Ph.D. thesis, University of Washington, Seattle, WA.
Jay, D. A. 1984 Circulatory processes in the Columbia River Estuary, final report, Columbia River Data Development Program, Astoria, OR.
Jay, D. A. 1987 Residual circulation in shallow stratified estuaries, Ph.D. thesis, University of Washington, Seattle, WA.
Jay, D. A. 1990 Tidal long wave propagation in channels of variable width and depth. *EOS*, **70** in press.
Jay, D. A., Giese, B. S. & Sherwood, C. 1989 Columbia River Estuary: energetics and sedimentary processes. *Progress in Oceanography* in press.
Jay, D. A. & Smith, J. D. 1988 Circulation, density structure and neap-spring transitions in the Columbia River Estuary. *Progress in oceanography* in press.
Lamb, H. 1932 *Hydrodynamics*, p. 279.
LeBlond, P. H. 1978 On tidal propagation in shallow rivers. *Journal of Geophysical Research* **83,** 4717–4721.
Levine, E. R. & Kenyon, K. E. 1975 The tidal energetics of Narragansett Bay. *Journal of Geophysical Research* **80,** 1683–1688.
Lighthill, M. J. 1978 *Waves in fluids*, Cambridge University Press, pp. 469.
Parker, B. B., 1984 Frictional effects of the tidal dynamics of a shallow estuary, Johns Hopkins University, Baltimore, MD.
Pearson, C. E. & Winter, D. F. 1977 On the calculation of tidal currents in homogeneous estuaries. *Journal of Physical Oceanography* **7,** 520–531.
Prandle, D. & Rahman, M. 1980 Tidal response in estuaries *Journal of Physical Oceanography* **10,** 1552–1573.
Proudman, J. 1952 *Dynamical oceanography* New York: Dover.
Sherwood, C. R., Jay D. A. Harvey, B. Hamilton P. & Simenstad, C. A. 1989 Historical changes in the Columbia River Estuary. *Progress in Oceanography* in press.
Snyder, R. L., Sidjabat, M. & Filloux, J. H. 1979 A study of tides, setup and bottom friction in a shallow semi-enclosed basin. Part II: Tidal model and comparison with data. *Journal of Physical Oceanography* **9,** 170–188.
Speer, P. E. & Aubrey, D. G. 1985 A study of non-linear tidal propagation in shallow inlet/estuarine systems. Part II: Theory. *Estuarine, Coastal and Shelf Science* **21,** 206–240.
Taylor, G. I. 1919 Tidal friction in the Irish Sea. *Philosophical Transactions of the Royal Society, London* **A,220,** 185–219.